ADVANCED MATERIALS
www.advmat.de

Versatile Carbon Hybrid Films Composed of Vertical Carbon Nanotubes Grown on Mechanically Compliant Graphene Films

By *Duck Hyun Lee, Ji Eun Kim, Tae Hee Han, Jae Won Hwang, Seokwoo Jeon, Sung-Yool Choi, Soon Hyung Hong, Won Jong Lee, Rodney S. Ruoff,* and *Sang Ouk Kim**

Substrate materials for carbon nanotube (CNT) growth have been mostly limited to brittle and flat dielectric oxide materials, such as Al_2O_3 and SiO_2.[1–6] An alternative substrate would (i) be stable at the moderately high temperatures needed for CNT growth, (ii) be mechanically compliant and stretchable for transfer to the widest array of base structures (flexible polymers, nonplanar structures, etc.), (iii) allow for the rapid and large-scale fabrication of complex device architectures, and (iv) if an electrically conductive substrate, would have Ohmic contacts at all junctions and similar work functions of CNT and the substrate, for efficient use of input electrical power. Thin films composed of overlapping nanoplatelets can satisfy either all four criteria or alternatively the first three criteria, if an electrically insulating substrate is desired. Options, thus, include a transparent and electrically insulating thin film that could be fabricated from overlapping nanoclay (vermiculite,[7] mica,[8] montmorillonite, etc.) platelets, overlapping hexagonal boron nitride platelets (as two examples) or, alternatively, for an electrically conductive substrate that is mechanically compliant, overlapping graphene-based platelets.[9,10] We have fabricated thin large-area films by deposition of graphene oxide platelets from aqueous colloidal suspensions, decorated them with patterned catalyst particles, and grown CNTs at exceptionally high growth rates and at temperatures that result in the substrate being converted to an electrically conductive graphene-based film.[2–4,9,11] Such carbon hybrid films have excellent flexibility and stretchability, can be readily transferred to any substrate including nonplanar surfaces, and were found to have Ohmic electrical contacts throughout the junctions in the CNT/metal-catalyst/"graphene-film" system. As examples, among many possible applications, the hybrid films were readily integrated into a field-emitting device and its excellent performance is reported herein.

Graphene is a one-atom-thick, two-dimensional layer of sp^2-hybridized carbons that possesses excellent mechanical,[9,10,12] electrical, and thermal transport properties.[13–20] Monolayer graphite, thus graphene, was originally synthesized on catalytic metal substrates by thermal chemical vapour deposition (CVD) and is the subject of extensive work since the 1970s in the surface-science community (also referred to as monolayer graphite (MG), rather than "graphene"; see references such as [21]). A breakthrough occurred in 2004 with several reports on the creation of graphene on insulating substrates, one method involving micromechanical exfoliation[21] to achieve thin layers on SiO_2-on-Si wafer pieces,[15] and another involving the growth of graphene by sublimation of Si from single-crystal SiC,[22] so that the transport physics could be studied without the interference of a conductive substrate in direct contact with the graphene.[15] An alternative to micromechanical exfoliation is the chemical production of graphene,[23,24] such as the exfoliation of graphite oxide by creation of a liquid dispersion, followed by deposition onto various substrates to yield thin films,[24] paper-like materials,[9] etc. For example, the ready dispersion of graphene oxide platelets in water allows for rapid deposition of highly uniform large-area films that, at the appropriate thickness, have good mechanical flexibility,[9] electrical conductivity,[23] and optical transparency.[25,26]

Figure 1a illustrates our method of making the CNT–graphene hybrid film. An aqueous dispersion of graphite oxide (i.e., containing suspended, individual graphene oxide platelets) is spin-coated onto a silicon wafer yielding a uniform film, composed of overlapping and stacked graphene oxide platelets, of about 7 ± 0.3 nm thickness, which, after thermal reduction, has a good electroconductivity as well as mechanical flexibility and optical transparency (Supporting Information, Fig. S1). Nanopatterned iron catalyst particles were deposited on this film surface by means of self-assembled block-copolymer nanoporous templates.[2–4,11,27–34] Figure 1b shows scanning electron microscopy (SEM) images of the uniformly sized catalyst islands upon the graphene film. The electron diffraction pattern of catalyst

[*] Prof. S. O. Kim, D. H. Lee, J. E. Kim, T. H. Han, J. W. Hwang, Prof. S. W. Jeon, Prof. S. H. Hong, Prof. W. J. Lee
Department of Materials Science and Engineering, KAIST
Daejeon 305-701 (Republic of Korea)
E-mail: sangouk.kim@kaist.ac.kr
Dr. S. Y. Choi
Convergence Components and Materials Laboratory
Electronics and Telecommunication Research Institute (ETRI)
Daejoen 305-700 (Republic of Korea)
Prof. R. S. Ruoff
Department of Mechanical Engineering and the Texas Materials Institute
1 University Station C2200
The University of Texas at Austin
Austin, TX 78712-0292 (USA)

DOI: 10.1002/adma.200903063

ADVANCED MATERIALS
www.advmat.de

www.MaterialsViews.com

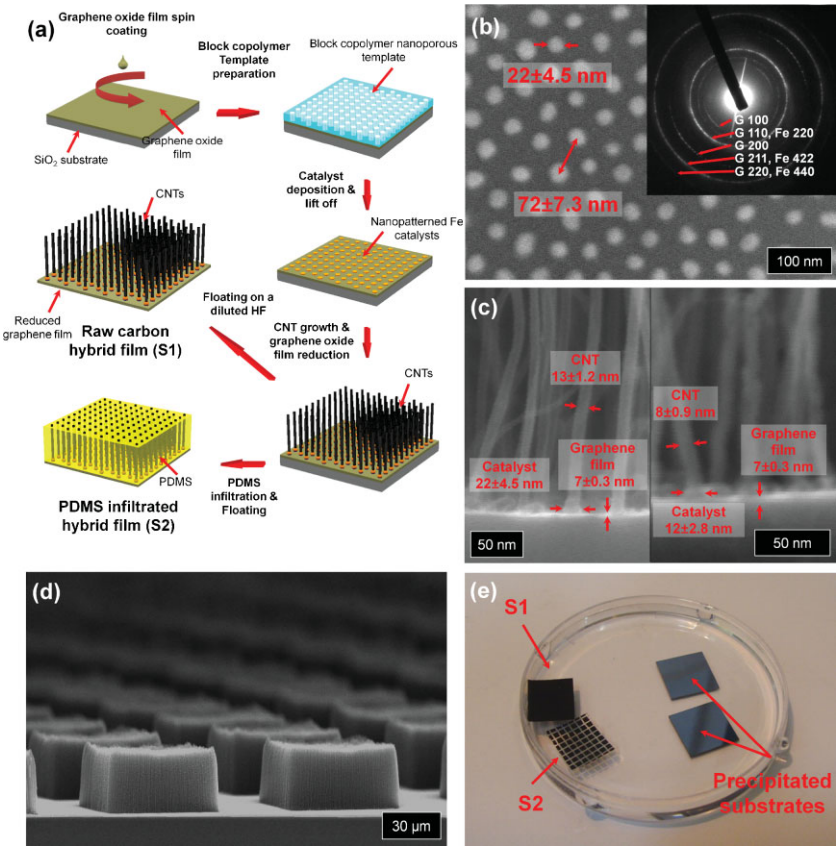

Figure 1. a) Schematic illustration of the fabrication process for carbon hybrid films. A multilayer graphene oxide film is spin-coated onto a SiO_2/Si substrate from an aqueous dispersion. The following block-copolymer lithography creates a nanopatterned iron catalyst array on the graphene oxide film. Highly aligned vertical CNT arrays are grown by catalytic PE-CVD. The underlying graphene oxide film is reduced and becomes electrically conductive during this high-temperature PE-CVD growth. The fabricated hybrid film with (S1) or without (S2) PDMS infiltration is detached from the Si substrate by wet-etching the SiO_2 layer. b) SEM image of iron catalyst particles on graphene film. The inset image shows the electron diffraction pattern. c) Cross-sectional SEM images of hybrid films. d) SEM image of a square-patterned CNT array on the graphene film. e) Photograph of S1 and S2 floating on a water surface.

particles obtained by transmission electron microscopy (TEM) matches that of a face-centered cubic (fcc) iron crystal.

Following preparation of the film with patterned iron catalyst particles, plasma-enhanced CVD (PE-CVD) growth of patterned CNTs was achieved at 600 °C under a flow of $C_2H_2/H_2/NH_3$ (5 sccm/80 sccm/20 sccm) at an overall pressure of 5 Torr, based on methods recently published.[2–4,11,35] The CNTs are doped with nitrogen (N-doped) and are primarily metallic. During the PE-CVD step, the underlying film composed of overlapping/stacked graphene oxide platelets is thermally reduced and has an electrical conductivity of about 1800 S m^{-1}. The electron diffraction pattern of the multilayer graphene film consists of concentric rings and not of individual spots and, thus, indicates a film of overlapping and reduced graphene platelets that are randomly oriented (Fig. 1b).

Figure 1c shows that the CNT diameter is precisely tunable by adjusting the catalyst particle size. As previously reported, our nanoporous templates of self-assembled block copolymer enables subnanometer-scale tuning of the particle size of the catalyst, such that highly selective growth of wall-number-selected CNTs is possible.[11] The fully grown carbon hybrid film, with CNTs having controlled heights ranging from 10 to 100 μm (Fig. 1d), were left as a raw hybrid film (S1) or infiltrated with a poly(dimethyl siloxane) (PDMS) elastomer (S2). The thickness of the PDMS infiltration was precisely controlled to expose the top ends of the CNTs (Fig. S2). Both PDMS-infiltrated hybrids and raw carbon hybrids were readily detached from the underlying silicon substrate by chemical etching (Fig. 1e). Owing to their mechanical flexibility, the hybrid films could be transferred onto nonplanar and/or flexible substrates indicating the critical role that the graphene film plays. Direct growth on nonplanar substrates, for example, could be very challenging depending on the substrate dimensions and, thus, its impedance match in a PE-CVD chamber and the fact that growth of wall-number-selected CNTs by our templating method is impossible on many types of nonplanar substrates. Growth of CNTs by PE-CVD or CVD at such high temperatures as 600 °C on flexible polymer substrates would be out of the question.

Therefore, we emphasize that the compliant substrate comprised of overlapped and stacked nanoplatelets that are also durable at high temperature in the presence of a variety of reactants such as for CVD or PE-CVD growth is a critical aspect, as was mentioned above. While others have emphasized the possibilities of reduced graphene oxide thin films on flexible polymer substrates,[18] we are here emphasizing the exceptional possibilities for new technology by using a thin graphene film as the substrate, which, at least with reactants that are not strong oxidants, will be stable to at least 1000 °C if not considerably higher.

We note that the vertical CNTs of PDMS infiltrated film can be macroscopically patterned in a square array, where the gap between the square CNT arrays looks transparent due to the optical transparency of the graphene film (Figure 1e).

In order to accomplish a successful catalytic growth of a densely packed vertical CNT array, catalyst shaping by thermal treatment is a crucial step.[11,36] This step is generally successful if the substrate material has a low surface energy. In addition, the catalyst particles should not be contaminated with the substrate material during the high-temperature CNT growth. Graphene is an outstanding substrate material for CNT growth due to its low surface energy and high thermal stability. Typically, CNTs grow to a length of 20 μm within 1 min and 100 μm within 10 min on the graphene-film substrates (Fig. S3).

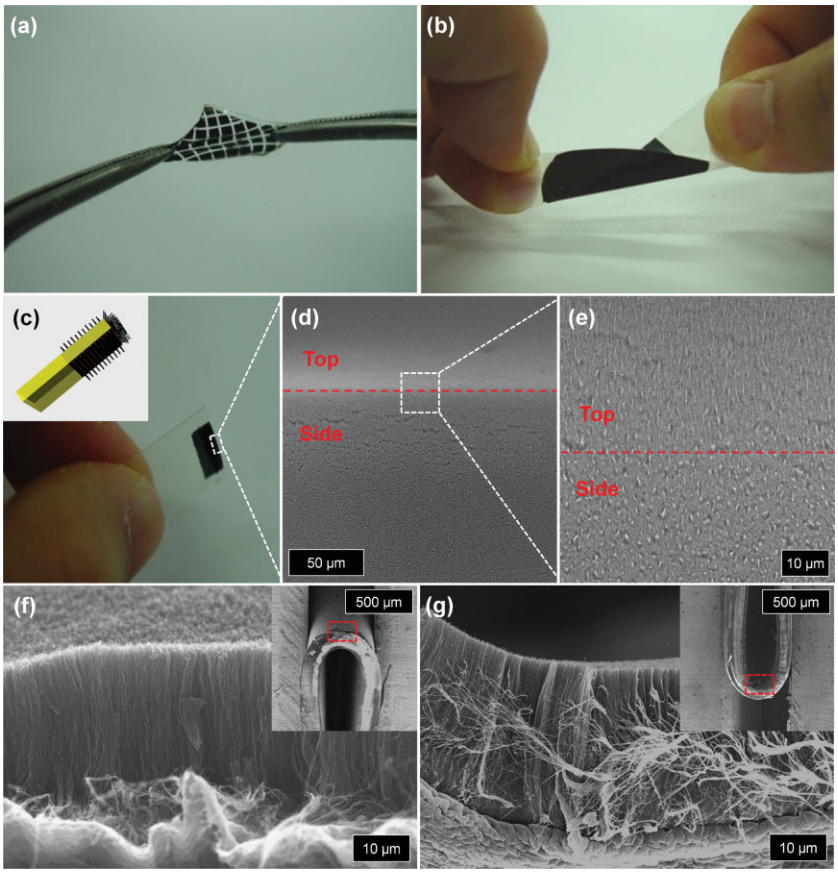

Figure 2. Photographs demonstrating: a) high stretchability/flexibility of S2 and b) extreme flexibility of S1 on a PET film. c) Photograph and d,e) SEM images of a hybrid film that encloses the PET film edge. High- and low- (inset) magnification SEM images of a carbon hybrid film on a PET film bent outward (f) and inward (g).

The carbon hybrid films demonstrated superb structural integrity during mechanical deformation of different types. Figure 2a shows that a PDMS-infiltrated film (S2) could be significantly stretched and bent without damage. As for neat PDMS films, the PDMS-infiltrated films could be repeatedly attached to and detached from nonplanar substrates (Fig. S2a). Figure 2b shows the high deformability of a raw hybrid film transferred onto a flexible poly(ethylene terephthalate) (PET) film. The film remains conformally contacted to the flexible PET film even when the PET film is highly deformed. The excellent mechanical compliance allows for rapid creation of highly nonplanar structures. Figure 2c shows a raw hybrid film conformally coating the edge of a thin PET film (thickness: ~130 μm). As shown in the magnified SEM images (Fig. 2d and 2e), the CNT forest morphology exactly follows the right-angle edge shape of the PET film. Figure 2Figures 2f and 2g show raw hybrid films that are highly bent on PET substrates. The hybrid films preserve their structural integrity and good contact with the PET film for both severe outward (Fig. 2f) and inward (Fig. 2g) bending. When the substrate is released, the hybrid film returns to their original planar shapes.

To quantitatively evaluate the impact of bending and stretching on the electrical conductivity, the electrical resistances of a graphene film and a hybrid film were measured under successive bending and stretching cycles, as was done previously for films composed of the CVD-grown, large-area graphene on flexible polymer substrates.[19] The variation in the normalized resistance for a 7-nm-thick graphene film on a PDMS substrate and of a PDMS-infiltrated hybrid film under successive bending cycles are shown in Figure 3a and 3b. Upon bending, the resistance of the graphene film increases at a radius of curvature of about 6 mm, probably due to changes in the relative positions of the individual platelets in the film (Fig. 3a). In contrast, the resistance of the PDMS-infiltrated hybrid film begins to increase at the much smaller radius of curvature of about 3 mm (Fig. 3b). The maximum increase in the normalized resistance for the PDMS-infiltrated hybrid film (~0.2%) is also much lower than that of the graphene film (~13%). When the samples are released from bending after a few cycles, both the graphene film and the PDMS-infiltrated hybrid film fully recover their original resistance values. After 1000 bending cycles, the resistance of the hybrid film increases by only about 1% (inset of Fig. 3b), demonstrating an extremely high structural stability. Figure 3c and 3d present the variations in the normalized resistance of the graphene film (Fig. 3c) and the PDMS-infiltrated hybrid film (Fig. 3d) under several stretching cycles. The resistance of the graphene film increases when the strain exceeds 15%, but up to a limiting strain of about 45% it fully recovers upon release, evidently due to the sliding of the overlapped and stacked reduced graphene oxide platelets in the film.[9,37] At 70% elongation the resistance exhibits a sharp increase and the zero-strain value is not recovered upon release, hence, the film fails (it "disintegrates") as can be seen by the naked eye. Owing to the high stretchability of the supporting graphene film, the PDMS-infiltrated hybrid can also be reversibly stretched up to the large strain of ~45% (Fig. 3d).

The electrical contact between the CNT forests and graphene film was measured for a PDMS-infiltrated hybrid film. Figure 4a and 4b show the electrical characterization by means of two-point-probe measurements and the obtained current–voltage (I–V) curves, respectively. Because each CNT forest is a square in the overall array, each square makes isolated contact. The I–V curves measured across the CNT forest/iron catalyst/graphene film (red curve in Fig. 4b) or the CNT forest/iron catalyst/graphene film/iron catalyst/CNT forest (green curve in Fig. 4b) show typical Ohmic response. The N-doped CNT forest shows Ohmic response and a work function of 4.27 ± 0.03 eV. The multilayer graphene film also exhibits typical Ohmic response (blue curve in Fig. 4b) and has a work function of 4.37 ± 0.03 eV

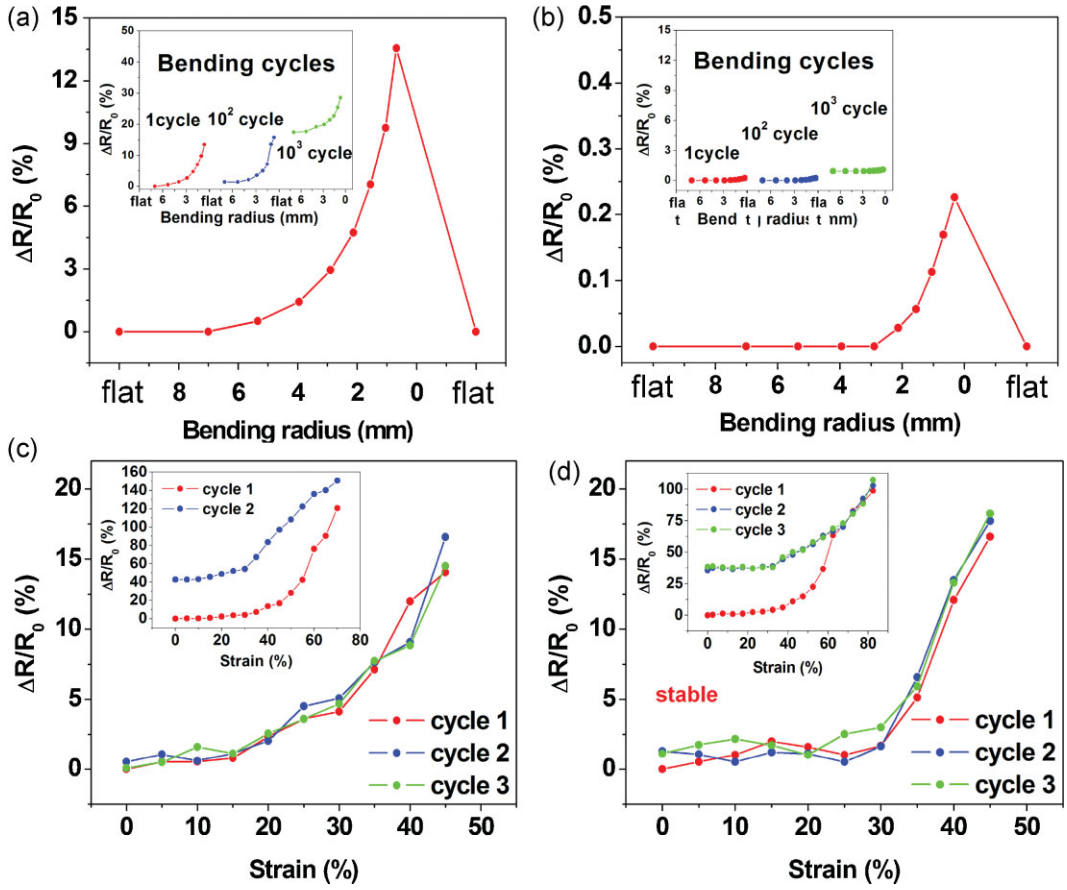

Figure 3. Resistance variations of: a) a graphene film on a 50-μm-thick PDMS substrate and b) a PDMS-infiltrated hybrid film (S2) as a function of bending radius. The insets show the results for the 1st, 100th, and 1000th cycle, respectively. Resistance variations of: c) a graphene film on a 50-μm-thick PDMS and d) a PDMS infiltrated hybrid film subjected to moderate (0 ∼ 45%) and large (0 ∼ 70%; inset) stretching.

(Fig. S1d). The work function of the iron metal catalyst is known to be 4.5 eV.[38] The system thus consists of Ohmic conductive components with work functions that range from 4.2 eV to 4.5 eV. As a consequence, all of the electric junctions are Ohmic without any significant barriers in resistance.

A hybrid carbon film floating on a water surface could be readily transferred onto a conductive substrate and integrated into a field emission device. We measured the room-temperature field-emission characteristics of hybrid films with different CNT wall numbers (CNT length: 40 μm for all films). Owing to the highly uniform CNT length and diameter as well as the stable electric contact to the underlying device substrate through the graphene film the emission is highly uniform over the entire film area (Fig. 4c). Figure 4d presents the variation in current density with the applied electric field. The turn-on field (measured at a current density of 10 $\mu A\,cm^{-2}$) decreases as the CNT wall number decreases (the CNT tip becomes "sharper"). The typical turn-on voltage for the double-walled CNTs exhibits an extremely low value of $0.4 \pm 0.06\,V\,\mu m^{-1}$, which is one of the lowest values reported for CNT-forest field emitters (Supporting Information, Table S1). The PDMS infiltrated film showed an increased turn-on field, presumably due to the limited number of exposed CNT tips at the top surface (see the reduced effective surface area in Table S1). The field emission from the highly uniform ensemble of CNT tips in these hybrid films can be fit with the Fowler–Nordheim equation over a broad voltage range.[39] The calculated field-enhancement factors (β) range from 9000 to 14500 (Fig. 4e). Moreover, the emission current showed a high reliability over one week of continuous operation (Fig. 4f). Owing to the uniform length and diameter and the low work function of the N-doped CNTs as well as the good electrical contact with the underlying graphene film, the mechanically compliant carbon hybrid films have excellent field emission.

The high temperature stability and mechanical compliance of films of overlapped nanoplatelets and the ready scalability to a very large area by straightforward deposition from colloidal suspensions (such as achieved commercially for paints, inks, etc.) suggest that the methods used here will be broad and versatile for fabricating not only CNT/graphene film hybrids but for the fabrication of a very wide array of materials on such thin and mechanically compliant films for transfer onto flexible and/or nonplanar substrates. This will be of great utility because there will be innumerable examples where such materials could not be directly prepared on the flexible and/or nonplanar substrates.[5,40]

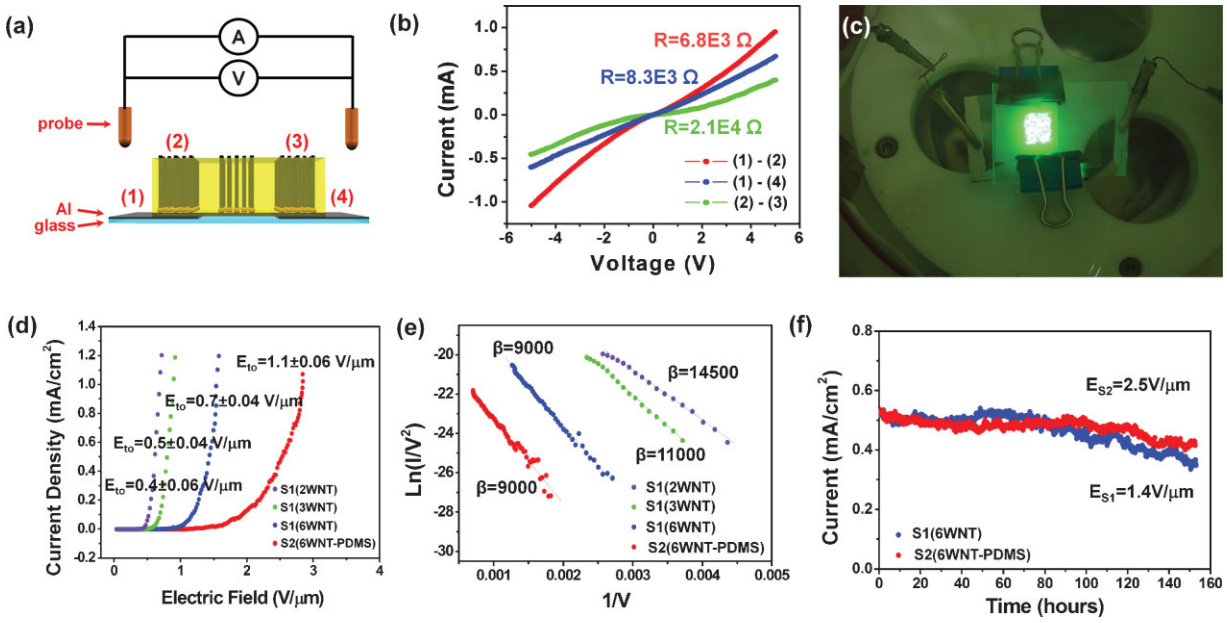

Figure 4. a) Schematic illustration of the electrical characterization of a PDMS-infiltrated hybrid film (S2) by the two-point-probe method and b) the measured *I–V* plots for various current paths. c) Photograph of a field-emitting device, d) current density versus electric field, and e) Fowler–Nordheim plots for the field emission of raw hybrid films (S1) with double- (2WNT), triple- (3WNT), and six-walled CNTs (6WNT) and a PDMS infiltrated film (S2) with six-walled CNTs at room temperature. f) Long-time reliability of carbon hybrid-film field emission.

Experimental

Carbon Hybrid-Film Preparation: First, an aqueous dispersion of graphene oxide was prepared using methods described elsewhere [9,23]. The average diameter of graphene oxide platelets was ~1.30 μm. A film comprised of overlapping and stacked graphene oxide platelets was prepared by spin-coating the aqueous dispersion onto a SiO_2 (500 nm)/Si wafer. Such spin-coated films were typically about 7 nm thick as measured in cross-section by SEM. Self-assembled nanoporous templates of block-copolymer thin film were prepared on the spin-coated film, using methods described elsewhere [9,24]. A film of iron particles was deposited onto the nanoporous block copolymer template. After complete lifting off of the block copolymer template by sonication, a nanopatterned iron catalyst particle array remained on the film. Vertical CNTs were grown from the nanopatterned catalyst array by PE-CVD. The graphene oxide film substrate was heated to 600 °C under a $C_2H_2/H_2/NH_3$ stream (5 sccm/80 sccm/20 sccm). When the substrate temperature reached 600 °C, the chamber pressure was fixed at 5 Torr and a 470 V direct current (DC) plasma was activated. Slow streaming of acetylene gas (5 sccm for 1 min to achieve, e.g., 20-μm-tall CNTs) resulted in vertical CNTs. During this high-temperature CNT growth, the underlying graphene oxide films were reduced and, thus, rendered electroconductive.

Field-Emission Measurements: A carbon hybrid film was transferred onto an ITO/glass substrate and an ITO/glass anode was positioned parallel to the top surface of the hybrid film. The spacing between the ITO anode and the top surface of the hybrid film was set to 500 μm. The field-emitting properties were measured under a vacuum of $\sim 10^{-6}$ Torr by applying a voltage of 0 V ~ 2000 V between the two electrodes.

Acknowledgements

This work was supported by National Research Laboratory Program (R0A-2008-000-20057-0), the World Class University (WCU) program (R32-2008- 000-10051-0), Basic Science Research Program (2009-0081359), the Pioneer Research Center Program (2009-0093758), and the Korea Science and Engineering Foundation (KOSEF) grant (R11-2008-058-03002-0) funded by the Korean government, and KAIST EEWS (Energy, Environment, Water, and Sustainability) Initiative (EEWS0903). R.S.R. was supported by NSF grants #CMMI-0802247 and #CMMI-0742065. Supporting Information is available online from Wiley InterScience or from the author.

Received: September 9, 2009
Revised: October 13, 2009
Published online: January 13, 2010

[1] K. Hata, D. N. Futaba, K. Mizuno, T. Namai, M. Yumura, S. Iijima, *Science* **2004**, *306*, 1362.
[2] D. H. Lee, D. O. Shin, W. J. Lee, S. O. Kim, *Adv. Mater.* **2008**, *20*, 2480.
[3] D. H. Lee, W. J. Lee, S. O. Kim, *Chem. Mater.* **2009**, *21*, 1368.
[4] D. H. Lee, D. O. Shin, W. J. Lee, S. O. Kim, *J. Nanosci. Nanotechnol.* **2008**, *8*, 5571.
[5] S. Talapatra, S. Kar, S. K. Pal, R. Vajtai, L. Ci, P. Victor, M. M. Shaijumon, S. Kaur, O. Nalamasu, P. M. Ajayan, *Nat. Nanotechnol.* **2006**, *1*, 112.
[6] Z. F. Ren, Z. P. Huang, J. W. Xu, J. H. Wang, P. Bush, M. P. Siegal, P. N. Provencio, Science. **1998**, *282*, 1105.
[7] D. G. H. Ballard, G. R. Rideal, *J. Mater. Sci.* **1983**, *18*, 545.
[8] *Functional Fillers and Nanoscale Minerals: New Markets/New Horizons* (Ed: J. J. Kellar), Society for Mining, Metallurgy and Exploration, Littleton, Colorado **2006**.
[9] D. A. Dikin, S. Stankovich, E. J. Zimney, R. D. Piner, G. H. B. Dommett, G. Evmenenko, S. T. Nguyen, R. S. Ruoff, *Nature* **2007**, *448*, 457.
[10] J. T. Robinson, M. Zalalutdinov, J. W. Baldwin, E. S. Snow, Z. Wei, P. Sheehan, B. H. Houston, *Nano Lett.* **2008**, *8*, 3441.
[11] D. H. Lee, W. J. Lee, S. O. Kim, *Nano Lett.* **2009**, *9*, 1427.
[12] C. Lee, X. Wei, J. W. Kysar, J. Hone, *Science* **2008**, *321*, 385.
[13] M. S. Dresselhaus, G. Dresselhaus, P. C. Eklund, *Science of Fullerenes and Carbon Nanotubes*, Academic Press, San Diego (CA, USA) **1996**.
[14] P. Avouris, Z. Chen, V. Perebeinos, *Nat. Nanotechnol.* **2007**, *2*, 605.

[15] K. S. Novoselov, A. K. Geim, S. V. Morozov, D. Jiang, Y. Zhang, S. V. Dubonos, I. V. Grigorieva, A. A. Firsov, *Science* **2004**, *306*, 666.
[16] L. Jiao, L. Zhang, X. Wang, G. Diankov, H. Dai, *Nature* **2009**, *458*, 877.
[17] Y. Zhang, Y. W. Tan, H. L. Stormer, P. Kim, *Nature* **2005**, *438*, 201.
[18] G. Eda, G. Fanchini, M. Chhowalla, *Nat. Nanotechnol.* **2008**, *3*, 270.
[19] K. S. Kim, Y. Zhao, H. Jang, S. Y. Lee, J. M. Kim, K. S. Kim, J. H. Ahn, P. Kim, J. Y. Choi, B. H. Hong, *Nature* **2009**, *457*, 706.
[20] S. Pang, H. N. Tsao, X. Feng, K. Mullen, *Adv. Mater.* **2009**, *21*, 1.
[21] X. K. Lu, M. F. Yu, H. Huang, R. S. Ruoff, *Nanotechnology* **1999**, *10*, 269.
[22] C. Berger, Z. Song, T. Li, X. Li, A. Y. Ogbazghi, R. Feng, Z. Dai, A. N. Marchenkov, E. H. Conrad, P. N. First, W. A. de Heer, *J. Phys. Chem. B* **2004**, *106*, 19912.
[23] S. Park, R. S. Ruoff, *Nat. Nanotechnol.* **2009**, *4*, 217.
[24] S. Stankovich, D. A. Dikin, G. H. B. Dommett, K. M. Kohlhaas, E. J. Zimney, E. A. Stach, R. D. Piner, S. T. Nguyen, R. S. Ruoff, *Nature* **2006**, *442*, 282.
[25] P. Blake, P. D. Brimicombe, R. R. Nair, T. J. Booth, D. Jiang, F. Schedin, L. A. Ponomarenko, S. V. Morozov, H. F. Gleeson, E. W. Hill, A. K. Geim, K. S. Novoselov, *Nano Lett.* **2008**, *8*, 1704.
[26] J. T. Robinson, M. Zalautdinov, J. W. Baldwin, E. S. Snow, Z. Wei, P. Sheehan, B. H. Houston, *Nano Lett.* **2008**, *8*, 3441.
[27] S. Park, D. H. Lee, J. Xu, B. Kim, S. W. Hong, U. Jeong, T. Xu, T. P. Russell, *Science* **2009**, *323*, 1030.
[28] R. D. Bennett, A. J. Hart, R. E. Cohen, *Adv. Mater.* **2006**, *18*, 2274.
[29] I. Bita, J. K. W. Yang, Y. S. Jung, C. A. Ross, E. L. Thomas, K. K. Berggren, *Science* **2008**, *321*, 936.
[30] S. O. Kim, H. H. Solak, M. P. Stoykovich, N. J. Ferrier, J. J. dePablo, P. F. Nealey, *Nature* **2003**, *424*, 411.
[31] S. J. Jeong, G. Xia, B. H. Kim, D. O. Shin, S. H. Kwon, S. W. Kang, S. O. Kim, *Adv. Mater.* **2009**, *20*, 1898.
[32] S. J. Jeong, J. E. Kim, H. S. Moon, B. H. Kim, S. M. Kim, J. B. Kim, S. O. Kim, *Nano Lett.* **2009**, *9*, 2300.
[33] B. H. Kim, H. M. Lee, J. H. Lee, S. W. Son, S. J. Jeong, S. M. Lee, D. I. Lee, S. W. Kwak, H. W. Jeong, H. J. Shin, J. B. Yoon, O. D. Lavrentovich, S. O. Kim, *Adv. Func. Mater.* **2009**, *19*, 2584.
[34] B. H. Kim, D. O. Shin, S. J. Jeong, C. M. Koo, S. C. Jeon, W. J. Hwang, S. Lee, M. G. Lee, S. O. Kim, *Adv. Mater.* **2008**, *20*, 2303.
[35] M. Chhowalla, K. B. K. Teo, C. Ducati, N. L. Rupesinghe, G. A. J. Amaratunga, A. C. Ferrari, D. Roy, J. Robertson, W. I. Milne, *J. Appl. Phys.* **2001**, *90*, 5308.
[36] D. N. Futaba, K. Hata, T. Namai, T. Yamada, K. Mizuno, Y. Hayamizu, M. Yumura, S. Iijima, *J. Phys. Chem. B* **2006**, *110*, 8035.
[37] S. Park, K. S. Lee, G. Bozoklu, W. Cai, S. T. Nguyen, R. S. Ruoff, *ACS Nano* **2008**, *2*, 572.
[38] H. B. Michaelson, *CRC Handbook of Chemistry and Physics*, 75th ed. (Ed: D. R. Lide), CRC press, London **1994**, Ch. 12.
[39] R. H. Fowler, D. L. Nordheim, *Proc. R. Soc. London* **1928**, *A119*, 173.
[40] A. Cao, V. P. Veedu, X. Li, Z. Yao, M. N. Ghasemi-Nejhad, P. M. Ajayan, *Nat. Mater.* **2005**, *4*, 540.